

Data Acquisition, Triggering, and Filtering at the Auger Engineering Radio Array

J. L. Kelley^a, for the Pierre Auger Collaboration^{b,1}

^a*Dept. of Astrophysics / IMAPP, Radboud University Nijmegen, 6500GL Nijmegen, Netherlands*

^b*Observatorio Pierre Auger, Av. San Martín Norte 304, 5613 Malargüe, Argentina*

Abstract

The Auger Engineering Radio Array (AERA) is currently detecting cosmic rays of energies at and above 10^{17} eV at the Pierre Auger Observatory, by triggering on the radio emission produced in the associated air showers. The radio-detection technique must cope with a significant background of man-made radio-frequency interference, but can provide information on shower development with a high duty cycle. We discuss our techniques to handle the challenges of self-triggered radio detection in a low-power autonomous array, including triggering and filtering algorithms, data acquisition design, and communication systems.

Keywords: radio, cosmic ray, AERA, Pierre Auger Observatory, self-trigger

1. Introduction

Cosmic-ray air showers emit coherent broadband radio pulses in the MHz frequency range, a phenomenon discovered by Jelley and collaborators in 1965 [1]. Advances in digital processing technology, along with the potential of the radio technique to determine cosmic-ray primary composition with a high duty cycle [2], have led to renewed interest in the technique [3]. Radio enhancements are now planned at several neutrino and cosmic-ray observatories.

Email address: j.kelley@astro.ru.nl (J. L. Kelley)

¹Full author list:

http://www.auger.org/archive/authors_2011_10.html

8 The goals of the Auger Engineering Radio Array
9 (AERA), a 20-km² extension of the Pierre Auger Observatory in Argentina,
10 are to calibrate the radio signal using hybrid air-shower measurements, and to
11 demonstrate the potential of the technique for future arrays. The first stage
12 of AERA is operational and is successfully measuring air showers of energies
13 at and above 10¹⁷ eV in coincidence with the Auger surface detector (SD) and
14 fluorescence detector (FD) [4].

15 **2. Detector and Data Acquisition Design**

16 The first stage of AERA, deployed in September 2010 and July 2011, consists
17 of 24 radio detector stations (RDSs) deployed on a triangular grid with a spacing
18 of 150 m and covering an area of ~ 0.4 km². Each RDS measures the radio signal
19 with a dual-polarization log-periodic dipole antenna (LPDA), aligned north-
20 south and east-west, and sensitive between 27 and 84 MHz. The received signal
21 is further amplified and bandpass filtered, and each polarization is digitized at
22 200 MHz with 12-bit analog-to-digital converters (ADCs). High-gain (+49 dB
23 after the antenna) and low-gain (+29 dB) versions of each channel are recorded
24 to extend the dynamic range.

25 A field-programmable gate array (FPGA) in the station electronics forms
26 a trigger when a bandwidth-limited pulse is observed in the voltage traces (a
27 “level 1” trigger). These triggers are passed to a CPU within the RDS, which
28 can then optionally apply other trigger conditions (the “level 2” trigger). The
29 triggers are timestamped using GPS receivers at each RDS.

30 The CPU in each RDS communicates via Ethernet over a fiber-optic net-
31 work to a central data acquisition system (DAQ). The RDS reports the trigger
32 timestamps to the central DAQ. The DAQ software forms the “level 3” trigger
33 by using time and spatial coincidences of multiple RDSs, and the time-domain
34 waveform data of these events is requested from each RDS and stored to disk.
35 Figure 1 shows the data flow for each trigger level.

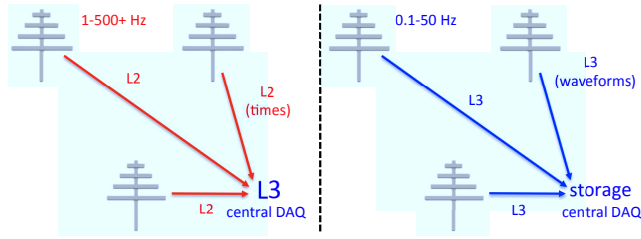


Figure 1: The AERA data flow. The GPS timestamps of station-level triggers (L2) are sent to a central DAQ, which forms multi-station coincidences (L3; shown at left). An L3 request is sent back to the stations (not shown), and digitized waveforms of the event are sent to the central DAQ for storage (shown at right).

36 **3. Triggering and Filtering**

37 Triggering directly on the radio signal of the air showers (instead of using particle
 38 detectors as a trigger) poses some challenges for the data acquisition, due
 39 to man-made radio-frequency interference (RFI). The continuous background
 40 level is set by the radio emission from the Galactic plane, but any man-made
 41 narrowband transmitters add to the level above which one must detect air-
 42 shower pulses. Additionally, man-made pulsed RFI (from sparking electrical
 43 equipment, airplanes, etc.) can mimic the signals from cosmic rays.

44 A comparison between raw level-3-triggered data and measured self-triggered
 45 cosmic-ray events is shown in Fig. 2. Since the bandwidth and computational
 46 resources at each triggering level are limited, one of the technical focuses for
 47 the first stage of the array has been to develop various methods to reject RFI
 48 in order to minimize efficiency losses from bandwidth saturation.

49 *3.1. Narrowband Filtering*

50 Before triggering on a radio pulse, it is advantageous to increase the signal-
 51 to-noise ratio by filtering out any narrowband transmitters from the digitized
 52 antenna signals. This is accomplished in a computationally efficient manner by
 53 using a series of infinite-impulse response (IIR) notch filters in the FPGA. The
 54 IIR filters operate on the time-domain signal, and the output of the filter y_i is
 55 a linear combination of input samples x_j and delayed feedback output samples

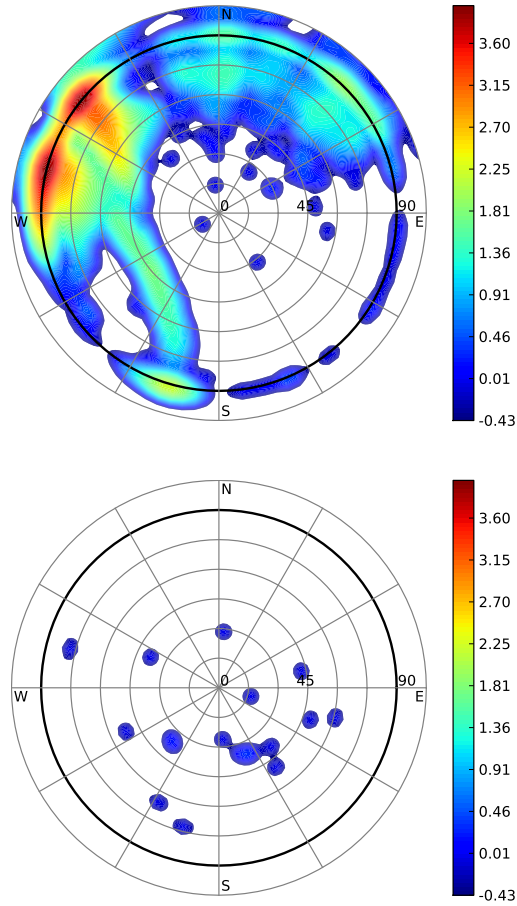


Figure 2: Top: unfiltered AERA polar skymap (2.5h, 40k events). The dark circle indicates the horizon. Bottom: AERA cosmic-ray events coincident with the Auger SD (48d, 18 events). The directions have been smeared with a 3° Gaussian, and the color scale is $\log_{10}(\text{event density, a.u.})$.

56 y_j from the filter:

$$\begin{aligned} y_i = & x_i - (2 \cos \omega_N \cdot x_{i-1}) + x_{i-2} \\ & + (2r \cos \omega_N \cdot y_{i-1}) - (r^2 \cdot y_{i-2}). \end{aligned} \quad (1)$$

57 The normalized filter frequency ω_N is given by the notch frequency f_N and the
58 sampling frequency f_S ,

$$\omega_N = 2\pi f_N / f_S, \quad (2)$$

59 and the width parameter r is a value strictly between 0 and 1, with higher
60 values giving a narrower response function. $r = 0.99$ is typical for a narrow
61 transmitter.

62 A complication in the implementation of the IIR filters in high-frequency
63 FPGAs arises from the fact that one cannot arbitrarily pipeline the feedback
64 computation. We have resolved this by using the scattered look-ahead pipelining
65 technique [5], which increases the filter complexity but allows more time for
66 computation in the FPGA.

67 The coefficients of the x_j and y_j in Eq. 1 can be precomputed for the desired
68 notch frequencies, converted to a fixed-point representation, and loaded into the
69 FPGA at run-time. The current design allows for four tunable notch filters for
70 each polarization. See Fig. 3 for an example of the filtering.

71 An additional filtering technique we are exploring is the use of a frequency-
72 domain median filter. The time-domain signal is first converted to the frequency
73 domain with a fast-Fourier transform (FFT), and then the amplitude of each
74 frequency component f_i is replaced by the median value in a window of size
75 $2N$: $\tilde{f}_i = \text{median}(f_{i-N}, \dots, f_{i+N})$. An inverse Fourier transform then converts
76 the signal back to the time domain for triggering. The median filter has the
77 advantage of removing any number of narrowband transmitters, but it is com-
78 putationally intensive and can distort pulse shapes in the time domain. The
79 pre-trigger FFT also allows for a number of other strategies for signal-to-noise
80 improvement, such as deconvolution of the filter dispersion, or use of a matched
81 filter [6].

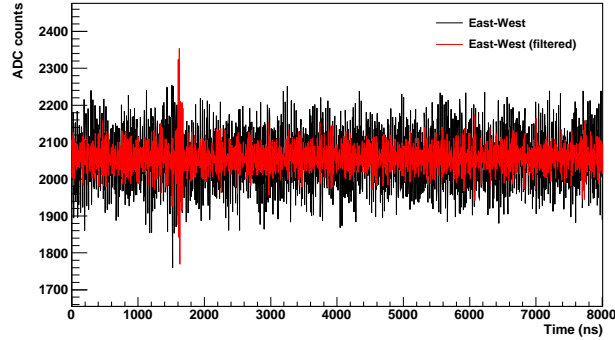


Figure 3: A recorded cosmic-ray radio pulse (at 1500 ns), before IIR narrowband filtering (black) and after (red, pulse offset in time). The peak signal-to-noise ratio increases from 2.4 to 7.6.

3.2. Level 1 Trigger

Designed to capture transient, isolated radio pulses, the digitizer uses algorithms in the FPGA to trigger in the time domain on potential signals. At its most basic, the trigger is simply a voltage threshold above a baseline. However, a number of other parameters are added to this trigger to reject RFI. The following trigger conditions are applied to select clean, bandwidth-limited pulses:

1. the voltage rising edge crosses the primary threshold T_1 ;
2. before the T_1 crossing, no other T_1 crossings occur during the previous time period T_{prev} ;
3. after the T_1 crossing, the signal rising edge crosses a secondary threshold T_2 ;
4. the number of rising-edge T_2 crossings NC within a time period T_{per} falls within a specified range $NC_{\text{min}} < NC < NC_{\text{max}}$;
5. the maximum time between successive T_2 crossings is less than TC_{max} ;
6. the quotient Q of the pulse maximum P_{max} divided by the number of T_2 crossings NC falls within the range $Q_{\text{min}} < Q < Q_{\text{max}}$.

The thresholds are compared relative to a baseline voltage, determined dynamically with a rolling average over a specified number of samples. Samples outside

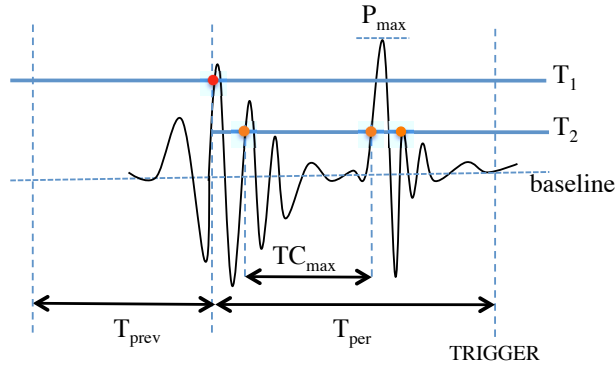


Figure 4: The AERA L1 trigger scheme. See the text for details.

101 of a specified voltage range (i.e. part of a large pulse) are not included in the
 102 baseline calculation.

103 Figure 4 shows the trigger parameters graphically. Each condition is de-
 104 signed to reject man-made RFI with specific characteristics. The quiet period
 105 T_{prev} rejects pulse trains. The secondary threshold T_2 , which is generally set
 106 lower than the primary threshold T_1 , rejects signals with after-pulsing, even if
 107 the after-pulsing is weaker than the initial pulse. The condition on the timing
 108 and number of T_2 crossings allows for some ringing of a bandwidth-limited pulse
 109 but rejects long and/or irregular pulse trains or digital spikes. The condition
 110 on $Q = P_{\text{max}}/NC$ can select on pulse shape, but in practice this is not needed
 111 when the other trigger parameters are set correctly.

112 Typical values for the thresholds and noise rejection parameters are as fol-
 113 lows: $T_1 = 200$ ADC counts and $T_2 = 150$ ADC counts, on an RMS noise level of
 114 40 ADC counts; $NC_{\text{min}} = 1$ and $NC_{\text{max}} = 8$ during a period of $T_{\text{per}} = 6.25 \mu\text{s}$;
 115 maximum crossing time TC_{max} of 130 ns; and a quiet pre-trigger period of
 116 $T_{\text{prev}} = 1.25 \mu\text{s}$.

117 The algorithm can trigger on either signal polarization, or the logical AND
 118 or OR of the two. The narrowband filtering described in Sect. 3.1 is performed
 119 before the trigger algorithm, but one can also trigger on the unfiltered signal;
 120 the unfiltered signal is stored in either case.

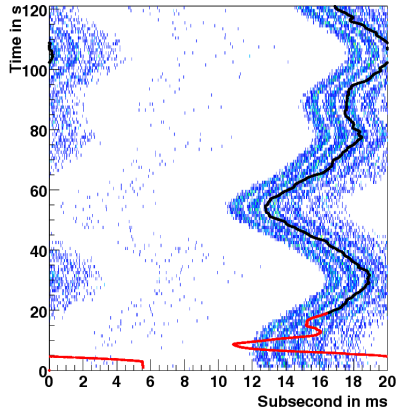


Figure 5: Sample L1 triggers, showing the residual from a 0.2 ms period (50 Hz) vs. time. The drifting phase can be tracked with a digital PLL (black line).

121 3.3. Periodicity Filtering

122 Man-made pulsed RFI, unlike cosmic-ray air showers, are often periodic in
 123 nature. In particular, by examining the time between successive level 1 triggers,
 124 clear signatures are visible at 100 Hz and sub-harmonics thereof (twice the power
 125 grid frequency of Argentina).

126 One difficulty in vetoing such events is the drift in phase of the 100 Hz pulses.
 127 This can be tracked in the RDS software with the use of a digital phase-locked
 128 loop, which can track the changing phase and allow a veto of the periodic events
 129 (see Fig. 5).

130 3.4. Directional Filtering

131 As shown in Fig. 2, most of the pulsed background events come from man-
 132 made sources on the horizon. When a level 3 trigger is formed with three or
 133 more stations in coincidence, the DAQ has enough information to reconstruct
 134 the direction and veto these events, either with a simple selection on the recon-
 135 structed zenith angle, or by using additional azimuthal and timing information.
 136 The only limitation is the computation time required for a directional recon-
 137 struction, which must keep up with the event rate. A plane-wave fit to the
 138 trigger times of the stations is sufficiently fast and accurate for such purposes.

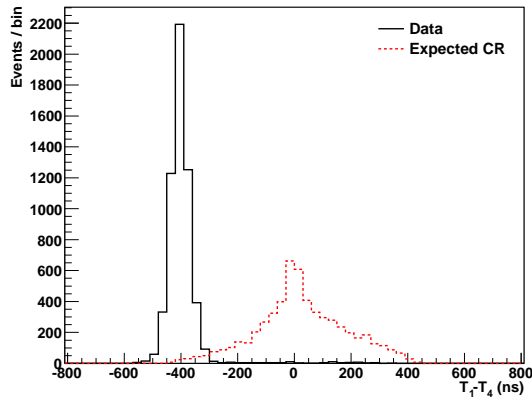


Figure 6: Trigger-time difference between stations 1 and 4 (solid: sample data, showing a pulsed RFI point source; dashed: expected cosmic-ray distribution, normalized to the same number of events).

139 A faster method that can veto directional hot spots, but does not require a
 140 full directional reconstruction, uses the distribution of trigger time differences
 141 between two stations. Directional hot spots can be identified by peaks in the
 142 time difference histograms for each station pair, and these distributions are quite
 143 different from that expected from air showers (see Fig. 6).

144 To remove the hot spots, the DAQ forms dynamic histograms $F(i, j)$ of
 145 trigger time differences $T_i - T_j$ for each station pair (i, j) ; the histograms con-
 146 tinuously update using a fixed number of past entries. For a candidate level 3
 147 trigger event, the number of “good” time differences (T_i, T_j) is calculated as

$$N_{\text{good}} = \sum_{N_{\text{pairs}}} \begin{cases} 1 & \text{if } F(T_i - T_j) < F_c \\ 0 & \text{otherwise} \end{cases}, \quad (3)$$

148 where F_c is an adjustable threshold that depends on the bin size and number of
 149 entries in the histograms. The selection criterion to keep the event is $N_{\text{good}} >$
 150 $N_{\text{pairs}}/2$. Future revisions may include the expected time distribution of air-
 151 shower events as well.

152 3.5. Offline Filtering

153 To date, confirmed cosmic-ray events in AERA have been found by searching
 154 offline for time coincidences with the water-Cherenkov surface detector of the

155 Pierre Auger Observatory. However, we are developing methods to identify
156 cosmic-ray candidates without information from other detectors.

157 One promising technique is the use of the signal polarization. Since the
158 primary component of the air-shower radio emission is geomagnetic in nature
159 [7], the direction of the predicted electric field \hat{e}_g is parallel to $\hat{v} \times \hat{b}$, where \hat{v}
160 is the direction of the shower axis, and \hat{b} is the direction of the local magnetic
161 field of the Earth. By deconvolving the response of the antenna and the station
162 electronics, the measured electric field of a radio pulse $\vec{E}(t)$ can be reconstructed
163 [8]. The direction of polarization can be compared to that expected from an air
164 shower with purely geomagnetic emission, i.e., events are selected if

$$\cos^{-1} \left(\hat{e}_g \cdot \frac{\vec{E}_{\max}}{|\vec{E}_{\max}|} \right) < \Psi_c , \quad (4)$$

165 where Ψ_c is a threshold space angle. This method does not yet account for
166 the contribution of secondary emission mechanisms with different polarization
167 signatures, such as that from the charge excess in the shower [9, 10]; however,
168 this can in principle be added using additional information such as the core
169 position of the shower.

170 4. Future Plans

171 AERA will expand in 2012 and 2013 to instrument an area of 20 km² with
172 160 radio detector stations. This expansion will entail a transition from com-
173 munication over optical fiber to a wireless network. Several designs are under
174 development for the wireless system, including:

- 175 1. a fully custom time division multiple access (TDMA) system in the 2.4
176 GHz band that supports up to 180 subscribers per channel, at a bandwidth
177 of 5.5 Mbps;
- 178 2. a commercial 802.11n + TDMA system in the 5 GHz band that supports
179 80-100 subscribers per channel, at a peak bandwidth of 150 Mbps (80
180 Mbps typical TCP/IP throughput); and

181 3. a distributed “gossip” protocol in which stations communicate with each
182 other and form multi-station coincidences without communication with a
183 central DAQ.

184 The first two systems are currently being field tested at the AERA site, while
185 the third system is in the development and simulation stage.

186 In addition to the developments in data acquisition, triggering, filtering, and
187 communications systems described here, the future stages of AERA will also
188 use enhanced antennas, low-noise amplifiers, and digitization hardware. The
189 increase in efficiency as well as detection area will result in a significant sample
190 of hybrid and super-hybrid events with which to quantify the potential of the
191 radio technique for measurement of cosmic-ray air shower energy, direction, and
192 primary composition.

193 **References**

- 194 [1] J. V. Jelley *et al.*, *Nature* **205** (1965) 327-328.
- 195 [2] T. Huege, R. Ulrich, and R. Engel, *Astropart. Phys.* **30** (2008) 96-104;
196 K. D. de Vries *et al.*, *Astropart. Phys.* **34** (2010) 267-273.
- 197 [3] H. Falcke *et al.*, *Nature* **313** (2005) 313-316.
- 198 [4] J. L. Kelley, for the Pierre Auger Collaboration, Proc. 32nd ICRC, Beijing,
199 China, 2011; arXiv:1107.4807.
- 200 [5] K. K. Parhi and D. G. Messerschmitt, *IEEE Trans. on Acoustics, Speech,*
201 *and Signal Processing* **37** (1989) 1099-1117.
- 202 [6] C. Ruehle, for the Pierre Auger Collaboration, *Nucl. Instrum. Meth. A,*
203 2010, in press, doi:10.1016/j.nima.2010.11.017.
- 204 [7] D. Ardouin *et al.* (CODALEMA Collaboration), *Astropart. Phys.* **31** (2009)
205 192-200; W. D. Apel *et al.* (LOPES Collaboration), *Astropart. Phys.* **32**
206 (2010) 294-303.

- 207 [8] P. Abreu *et al.* (Pierre Auger Collaboration), Nucl. Instrum. Meth. A **635**
208 (2011) 92-102.
- 209 [9] H. Schoorlemmer, for the Pierre Auger Collaboration, Nucl. In-
210 strum. Meth. A, 2010, in press, doi:10.1016/j.nima.2010.11.145.
- 211 [10] V. Marin, for the CODALEMA Collaboration, Proc. 32nd ICRC, Beijing,
212 China, 2011.